

ENERGETIC CONDENSATION GROWTH OF NIOBIUM FILMS

M. Krishnan, I. Irfan, Alameda Applied Sciences Corporation, 3077 Teagarden Street, San Leandro, CA, USA,

T. Tajima, Los Alamos National Laboratory, Los Alamos, New Mexico, USA,

T. Proslie, Argonne National Laboratory, Argonne, IL, USA,

R. Geng, P. Kneisel, C. Reece, X. Zhao, Thomas Jefferson National Accelerator Facility, Newport News, VA 23606, USA

Abstract

Energetic Condensation refers to thin film growth on a surface using ~ 100 eV ions, versus lower energy deposition using sputtering (~ 1 -10 eV with no substrate bias) or still lower energy thermal evaporation. The relatively high incident energy of energetic condensation creates defects and vacancies within the first few atomic layers and enables diffusion to lower free-energy sites in the lattice. Shallow defects migrate to the heated surface and are annihilated, leading to low-defect crystal growth. It has been shown [1] that the purer the film, the closer are its superconducting parameters to those of the bulk metal. Use of cathodic arc plasmas was proposed in 2000 by Langner [2] followed by detailed development of the process [3]. AASC's work in this area has picked up from the European Community-Research Infrastructure Activity and has demonstrated very high RRR=541 in Nb films grown on crystal substrates [4]. The physics of energetic condensation and work in progress to coat 1.3 GHz copper cavities using cathodic arc plasmas are described.

INTRODUCTION

In the early 1980s, researchers at CERN [5] explored the concept of sputtered films of Nb on copper cavities as a potential replacement for bulk Nb SRF cavities. Q_0 values in excess of 2×10^9 at 5 MV/m were reproducibly achieved on single cell 500 MHz cavities and a Q_0 value of 6.2×10^9 was reached at 5 MV/m on a 4-cell 352 MHz cavity. These excellent results were somewhat tempered by the sporadic appearance of blisters in the Nb film and a rapid decrease of Q_0 with increasing field. Papers published in the 1990s [6, 7] suggested that impurities in the film were responsible for the drop in Q with higher field. In the early 2000s, Langner [2], Russo [3] and others proposed the use of cathodic arcs to grow the Nb thin films. This pioneering work was motivated by the fact that cathodic arcs naturally generate ions that are energetic (40-120 eV) vs. the ~ 1 eV ions from magnetron guns. The more energetic ions would presumably lead to denser (less porous) films with better adhesion. Furthermore, the source of ions from an ultrahigh vacuum might also be conducive to purer films with better SRF properties. Residual Resistivity Ratio (RRR) of up to 100 was measured in Nb films grown at substrate temperatures of ~ 100 °C. RF cavity cells were coated using various configurations of cathodic arcs.

Our work using cathodic arcs picks up where the European work under the program CARE (Coordinated Accelerator Research in Europe for particle physics) left off, in about 2006 [8, 9].

This paper begins with a brief description of the physics of energetic condensation. There are three types of plasma sources that use energetic ions to grow thin films: cathodic arcs, electron cyclotron resonance (ECR) sources and High Power Impulse Magnetron Sputtering (HiPIMS). All three sources produce dense, well adhered films and have therefore been actively pursued for better SRF cavity coating applications. This paper presents results using cathodic arcs. Our earlier work on coupons of A-plane a-sapphire and MgO [4] motivated coating of Nb films on Cu coupons and has recently progressed to coating 1.3 GHz elliptical-cell RF cavities. Some preliminary results of the cavity coatings are described in this paper.

ENERGETIC CONDENSATION

A cathodic arc plasma uses a low voltage (~ 30 V) arc discharge to generate a highly ionized plasma, the ions of which consist exclusively of the cathode material. The plasma is created in a vacuum arc discharge, so can be sustained in ultrahigh vacuum ($\sim 10^{-8}$ Torr) conditions. For Nb plasmas, the ion energy spectrum has been measured [10] to lie in the range of 60–120 eV, with most of the ions being triply charged. When such energetic ions impinge in the normal direction upon a substrate, they penetrate and deposit their energy within a few monolayers from the surface. The net energy deposited is in the range of 100–170 eV, as the ≈ 46 eV of ionization potential energy carried by Nb^{3+} is added to the kinetic energy. This energy greatly exceeds typical binding energies in the lattice (~ 10 eV), so substrate atoms are displaced and the excess energy goes into electronic and phonon excitations. These ion deposition processes occur on a rapid time scale of < 1 ps. This time scale may be estimated as follows: the range of Nb ions in sapphire or MgO substrates is ~ 1 nm (a few monolayers). The fastest incident ions with ~ 14 km/s speeds (100 eV energy) that are stopped after a single binary collision in the lattice would travel for $\sim 1 \text{ nm} / 14 \text{ km/s} \approx 70$ fs. Slower ions moving at ~ 4 km/s (10 eV) and suffering many inelastic collisions before stopping might cover a distance of ~ 3 nm and thus take 0.75 ps. Lifshitz et al. [11] and Brice et al. [12] have described the details of the interaction

between energetic ions (~100 eV) and various substrates. They have coined the term “subplantation” to distinguish this regime of ion-surface interactions from deep implantation (>1 keV ions) and surface interactions (<1 eV). In subplantation, the incident ions deposit more than enough energy into just a few subsurface atomic layers to displace atoms from the lattice and create interstitials. The key to effective subplantation is to maximize the number of displacements within this subsurface layer, while minimizing deeper defects. This is because the ion energy deposition (that occurs on ~1 ps time scales) must be accompanied by substrate heating. This heating allows subsurface defects (lattice dislocations, voids and impurities) to migrate to the surface where they are annihilated. Such a synergistic interplay between the highly non-equilibrium ion deceleration physics in the top few atomic layers and thermal diffusion physics in the bulk, promotes growth of the film in a low energy state that is likely to be epitaxial growth, evolving as the film thickens, to homo-epitaxial growth. Our pulsed discharge is fired once every few seconds, so the synergistic effects of fast ion deposition and thermal annealing are completed on each pulse.

Anders [13] has suggested a revision of the classical Thornton diagram [14] in which he replaces the gas pressure axis of Thornton’s with an ion energy axis. Anders suggests that energetic condensation allows the film to develop properties that in a thermal environment would require substrate temperatures that approach melting, i.e. a so-called homologous temperature of near unity. Here we mention another way in which to look at the effect of energetic condensation: highly localized heating of the substrate to melt, followed by very rapid cooling. N.A. Marks [15] provides a simple estimate of the heating due to ion stopping in a solid. The initial radius of the spike created by the stopped ion is estimated by equating the ion energy E_{ion} with the amount of kinetic energy in a hemisphere of radius r_0 at the melting temperature of Nb of 2742K:

$$E_{ion} = \rho kT * \frac{2}{3} \pi r_0^3 \quad (1)$$

For the typical 100 eV Nb ion in energetic condensation, this radius is 1.48 nm. There are ~100 atoms in the substrate that are affected by a single incident ion into the lattice. The mobility of the quasi-liquid atoms in the spike at a thermal speed of ~700 m/s implies a time of ~0.5 ps to cover one lattice spacing. We may regard the displacement time scale in the disturbed lattice as ~0.5 ps. Next (following Marks) we estimate the time scale for cooling of the local hot spot by thermal diffusion into the undisturbed lattice. Marks uses separation of variables to derive a simple analytical expression for the heat diffusion in terms of Bessel functions that are easily evaluated for the conditions of our experiment.

Figure 1 shows a schematic representation of the diffusion cooling in a Nb film. Although the substrate might be copper, since the relevant length scales are ~1 nm, and since the typical film is ~1000 nm, these physical

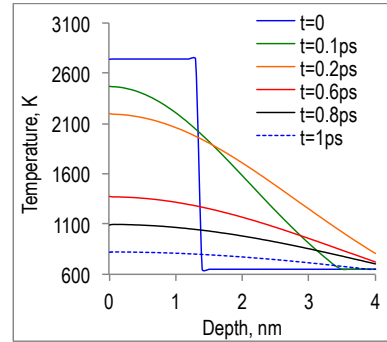


Figure 1: Schematic representation of quenching of the 1.5 nm radius, hemispherical hot spot by diffusion cooling

processes take place in Nb, so the thermal conductivity, density and specific heat of Nb were used in the analysis. It was found that after ~0.8 ps, the temperature of the local hot spot is quenched to “1/e” of the melting temperature, when any rearrangement of atoms in the lattice should cease.

The similarity of these time scales: for lattice rearrangement and rapid quenching of the mobility, imply that each incident energetic ion disturbs ~100 atoms in the lattice and allows significant rearrangement of the lattice within the ~1.5 nm hemispherical range of influence. For greater precision, a Monte Carlo calculation (such as TRIM) should be used to track the detailed slowing down of the incident energetic ion, taking into account angles of incidence and straggling. Nevertheless, the simple estimates provide a physical picture of the dominant process and gives insight into how energetic condensation differs from lower energy deposition processes such as sputtering or PVD. The basic tenets of Brice et al.’s [12] definition of sub-plantation: that the energy be deposited into a few monolayers and that the ratio of surface to bulk defects be high, are met in the case of Nb deposition onto a heated copper substrate. Brice examined ion bombardment of silicon in the context of semiconductor thin film growth. We have adapted his ideas for our case. In the case of either the vacuum arc or the ECR, the energy is easily varied by varying the substrate bias voltage. But there are subtle differences in the ion spectra. The coaxial energetic deposition (CED) spectrum is broad and ranges from ~60 eV up to ~170 eV, whereas the ECR spectrum would be a more narrow spectrum with only a ~10 eV spread about the mean. Then too, the angular spread of the incident ions is also important as the range of ions in the solid varies strongly with angle.

CED APPARATUS

Figure 2 shows a photograph of the Coaxial Energetic Deposition (CED) apparatus. Base pressures of ~10⁻⁸ Torr are possible within this chamber and are measured and monitored using a SRS200 residual gas analyser. In addition to substrate temperature control, the substrate can also be biased. The key process variables are substrate temperature, degree of annealing, substrate bias,

deposition rate, and base pressure. The principle of CED operation is shown on figure 3.

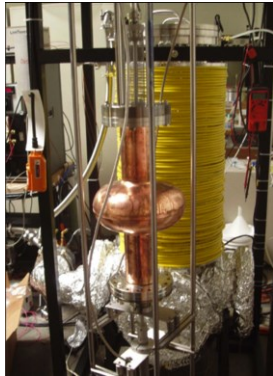


Figure 2: Photograph of the CED apparatus, with a 2.2 GHz RF cavity shown for scale.

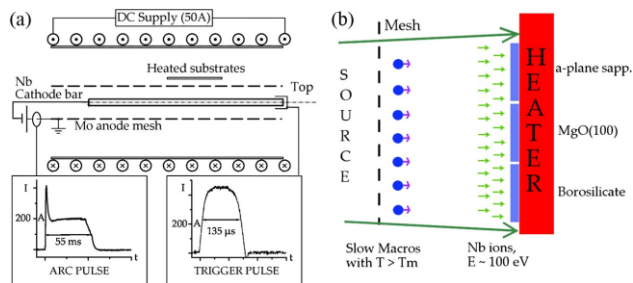


Figure 3: Schematic drawing of CED operation: (a) coaxial electrode geometry and typical current pulses to trigger an arc; (b) detail of anode mesh and heated substrate, showing plasma transmitted by the anode onto the substrate.

Estimate of Instantaneous Deposition Rate

The erosion rates from cathodic arcs of almost all metallic elements in the periodic table have been measured by several researchers over decades of study. Recent books by Boxman [16] and Anders [17] summarize these data. A reasonably good estimate for Nb is 30 μg/C. It is also well known that current from cathodic arcs flows from tiny spots ~1μm in diameter, each carrying ~80-100 A. For our ~150 A CED arc, there might be just one spot or at most two spots that carry the current. The plasma from this spot is highly ionized and explodes outwards into the vacuum with a directed speed of ~12 km/s. At a short distance from the spot, the plasma has a kinetic temperature of ~3-4 eV, consistent with a mean charge in Nb of 2+. The ion thermal velocity at these temperatures is ~3 km/s. The conical expansion of the hot plasma from the spot is akin to a supersonic flow from a nozzle with a Mach number of 4 (12 km/s)/(3 km/s). A rule of thumb for such an expansion is that the cone angle θ (the cone within which >90% of the flow is contained) is given by:

$$\theta = \sin^{-1}\left(\frac{1}{M}\right) \quad (2)$$

We may approximate the expansion as into a cone of half angle 14°. Measurements were made of the axial and

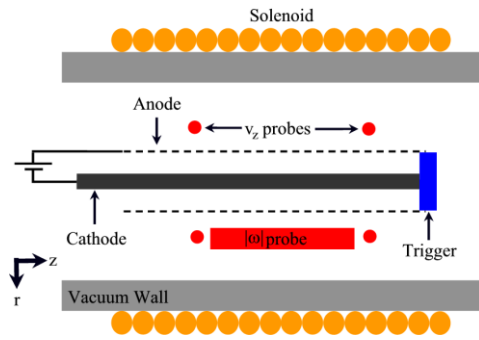


Figure 4: Configuration of Langmuir probes used to measure the axial velocity of the spoke (rings spaced 14cm apart) and the angular rotation (0.25'' dia. rod at 5 cm radius from axis).

angular velocity of the arc spoke in the CED geometry. Figure 4 shows the probe configuration used for the measurements. The arc spoke in the CED executes a helical motion as it runs down the Nb cathode from the trigger zone (in blue in the figure) to the power supply end of the rod. Two electric probes (SS304 0.025'' diameter wire) in the shape of rings allowed the axial velocity to be measured by time-of-flight, while a single 0.25'' diameter SS304 rod connected to ground through a Pearson Coil (red rod in figure) measured the angular speed by registering the spoke each time it whipped around the axis and made impact with the rod.

At axial magnetic field strengths of ~5-10 mT, the

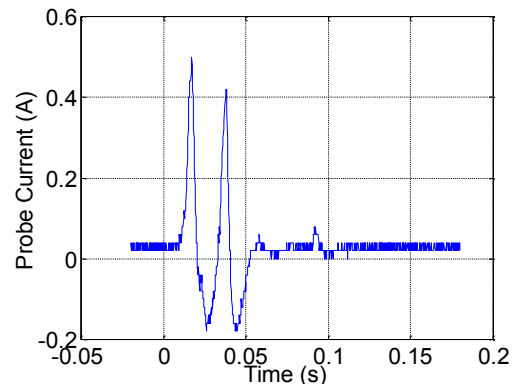


Figure 5: Time-of-flight separation of two axial probes spaced 14 cm apart.

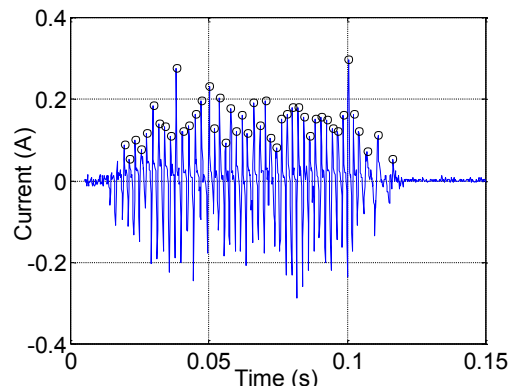


Figure 6: Angular rotation velocity of arc spoke measured using the 0.25'' diameter rod (Fig. 4).

measured axial speed was 6-8 m/s (see Fig. 5) while the angular rotation frequency (see Fig. 6) was $\sim 3\text{-}4 \times 10^3$ rad/s.

These values define the helicity of the spoke motion. The rotation period is 2.1 ms (for $\omega = 3 \times 10^3$ rad/s). The transit time to cover the 40 cm length of the Nb rod is ≈ 50 ms. Thus the spoke executes ≈ 20 orbits as it flies down the cathode. The pitch of the helix is ≈ 2 cm. Such a pattern of damage was observed on the cathode after just a few shots. With coating runs of 1000's of shots, the random initiation of the spots at the trigger end eventually wash out any signature of the helix, as expected.

Tables 1 and 2 show the steps used to estimate the instantaneous deposition rate.

Table 1: Spot Radius and Dwell Time of Arc on Spot

when substrate radius=	3	cm
spot radius=	0.76	cm
omega=	3.00E+03	rad/s
tau=	2.1	ms
angular velocity=	90	m/s
dwell time on spot=	1.68E-04	s

Table 2: Instantaneous Deposition Rate

erosion rate=	3.00E-05	g/C
current=	150	A
m_dot @cathode=	4.50E-03	g/s
anode transmission=	60%	
m_dot @substrate=	2.70E-03	g/s
flux @substrate=	1.50E-03	g/cm ² -sec
fluence on given spot=	2.52E-07	g/cm ²
film thickness on spot=	0.294	nm
inst. dep. rate=	1745	nm/s

First consider Table 1: take the case for a substrate at 3 cm radius (the beam tube of a ~ 1 GHz cavity, for example). For the expansion angle given by Eq. 1, the spot radius at the substrate location is 7.6 mm. The angular rotation frequency gives an angular velocity at this radius of 90 m/s. Hence the spot traverses its own footprint in $(2 \times 0.76 \text{ cm} / 90 \text{ m/s}) = 168 \mu\text{s}$.

Next consider Table 2: start with the erosion rate for Nb at these currents of $30 \mu\text{g/C}$. The arc current of 150 A gives a mass flow rate out of the cathode at the spot of 4.5 mg/s. The anode transmission of 60 percent and the spot area give the flux at the substrate location of $1.5 \text{ mg/cm}^2\text{s}$. From the last row in Table 1, we calculate the fluence at the substrate as $0.252 \mu\text{g/cm}^2$. With the density of Nb of 8.57 g/cc , we get the film thickness/pulse at the substrate as $\approx 3 \text{ \AA}$, or one monolayer/pulse. The last row in Table 1 gives the instantaneous deposition rate as 1745 nm/s. The spot diameter is 1.5 cm whereas the pitch of the helix is ≈ 2 cm. At small radial distances from the axis, the spot does not fully cover the cavity surface as it rotates down the cathode. However, at a radius of 10 cm from the axis (equator of cavity) the spot diameter has expanded to 5 cm which is larger than the pitch. Thus a given zone of the cavity surface sees the spot twice during

one pulse i.e. there is overlap. It is easy to show that the fluence in a cylindrical geometry falls off as $1/r$, where r is the radial distance from the axis, not as $1/r^2$, as is the case for a single spot expanding freely into vacuum. Therefore the instantaneous deposition rate at the equator is $\approx 500 \text{ nm/s}$.

RF CAVITY COATING

Prior publications [4, 18] have described high RRR (up to $\text{RRR}=541$) measured from Nb films deposited on various crystal substrates. Those results motivated coating of RF cavities for tests at cryogenic temperatures.

Figure 7 (left) shows a photograph of the KEK-03 1.3 GHz cavity that was supplied by LANL and coated using the CED apparatus. The image at right shows the interior after coating. The coating was achieved using 13,500 pulses at a cavity temperature of $330 \text{ }^\circ\text{C}$ (measured half way down the beam tube). The estimated film thickness is $\sim 5 \mu\text{m}$ in the beam tube and $\sim 1.5 \mu\text{m}$ at the equator.

Figure 8 shows the Q_0 vs. E_{acc} graph of this cavity (measured at LANL) at 4 K and 2 K as noted in the legend. The lack of difference between 4 K and 2 K results suggests that losses are due to beam-pipe flanges, not the cavity itself. This was confirmed by measuring the cavity with the flanges coated with Nb as shown in Fig. 8. The beam pipe length of 120 mm was determined to be too short for a negligible loss on the flanges.

The KEK-03 cavity was rinsed using a high pressure water rinse (HPWR) in a clean room environment at LANL. Figure 9 shows photographs of the coated cavity before the rinse (left) and after the rinse (right). The Nb film was well adhered and survived the HPWR test.



Figure 7: KEK-03 cavity (left) and interior image after coating (right).

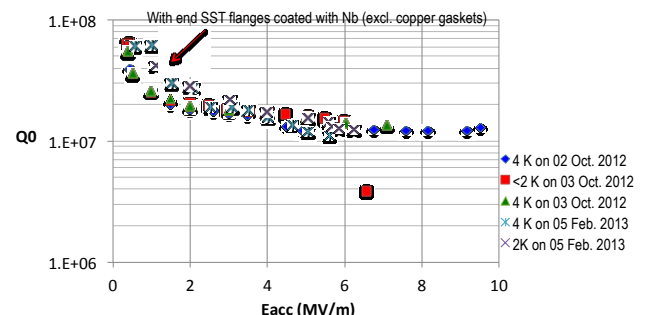


Figure 8: Q_0 vs. E measurements from KEK-03 cavity at 4 K and 2 K.

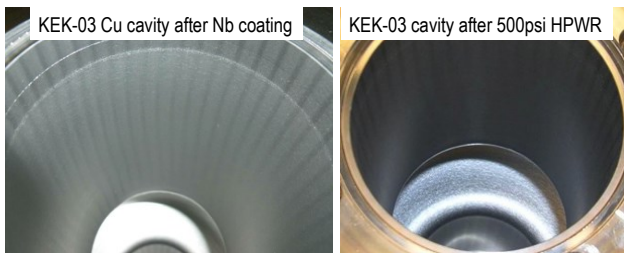


Figure 9: Photograph of KEK-03 cavity coated with Nb (left) and after ~500 psi high pressure water rinse (right).

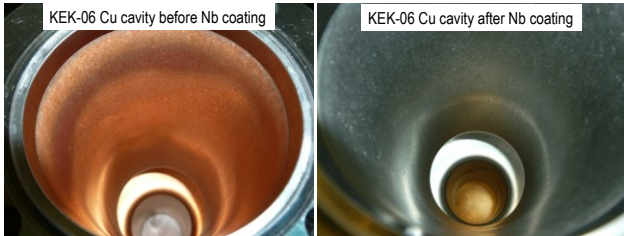


Figure 10: Photograph of KEK-06 cavity as received (left) and after coating with Nb (right).

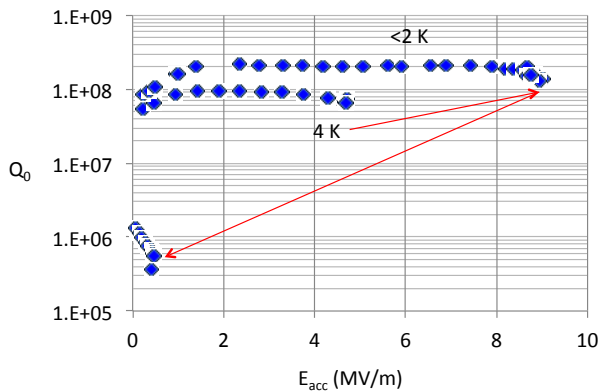


Figure 11: Q_0 vs. E_{acc} measurements from KEK-06 cavity at 4 K and <2 K.

Figure 10 shows photographs of the KEK-06 cavity (with 50 mm longer beam pipes) before (left) coating and after (right) coating. This coating run used 12,000 shots with the cavity at 350-360 °C to produce a Nb film of similar thickness to that of KEK-03.

Figure 11 shows the Q_0 vs. E_{acc} graph of this cavity (measured at LANL) at 4 K and <2 K.

This cavity does show a difference between 4 K and 2 K probably because we eliminated the effect of the end flanges, by making them longer than for KEK-03. The difference is, however, much smaller than what one would expect, i.e., BCS resistance should be about 40x less if all the surfaces were Nb. This result suggests that there are areas that are not coated well and lossy, which is causing the lower than expected Q_0 . A temperature mapping system is required to locate the zones that are lossy.

Figure 12 shows photographs of the next Cu cavity that was coated, provided by ANL. This cavity was tested at JLab by P. Kneisel. Unfortunately, the results were not encouraging. The cavity was superconducting but with a

low-Q at 4 K and only minor improvement at 2 K. The one encouraging observation from these tests was that despite several cycles of High Pressure Water Rinse (HPWR) the Nb coating has held up rather well.

Our next improvement planned for the CED apparatus is implementation of a macro-particle filter that consists of alternate vanes as shown in Figure 13.

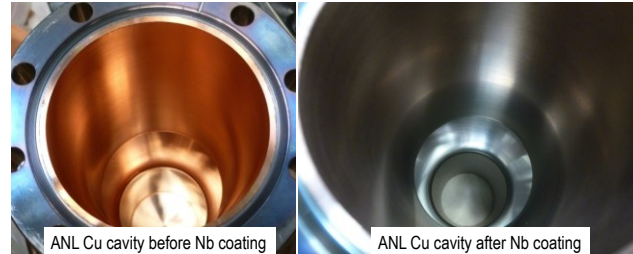


Figure 12: Photographs of ANL Cu cavity as received (left) and after coating with Nb (right).



Figure 13: CED electrode configurations: unfiltered (left); vane filtered (middle); expanded view of vane filter (right).

The expanded view of the vane filter (right) shows that by driving the current (either the arc current itself or else an external current) one can create a local magnetic field between vanes that would guide the fully ionized plasma around the vane structure and into the vacuum gap towards the cavity walls, whilst blocking the uncharged macro-particles, that would now have no direct line of sight to the cavity walls.

SUMMARY

We have described the mechanism of energetic condensation growth of Nb films and have presented a simple physical model for such film growth. Building upon our prior accomplishments with small coupons, here we have presented recent results of coated 1.3 GHz single-cell elliptical cavities made of copper. The highest gradient so far has been about 9.5 MV/m limited by the available RF power due to significantly low Q_0 , suggesting non-uniform coating with some normal conducting spots. The next step will be to identify the areas of inadequate coating and optimize coating parameters to improve the coating quality to improve the Q_0 .

ACKNOWLEDGMENT

This research is supported at AASC by DOE via Grant No. DE-FG02-08ER85162 and Grant No. DE-SC0004994. We sincerely thank Colt James for his earlier contributions to this research. We also would like to thank KEK for providing hydroformed copper cavities through their collaboration with LANL.

REFERENCES

- [1] C. Benvenuti et al, IEEE Trans. Appl. Supercond. 9 (1999).
- [2] J. Langner, TESLA Rep. 2000-15, D. Proch, DESY 2000.
- [3] R. Russo et al, Supercond. Sci. Technol. 18 (2005) L41-L44.
- [4] M. Krishnan, E. Valderrama, B. Bures, K. Wilson-Elliott, X. Zhao, L. Phillips, Anne-Marie Valente-Feliciano, Joshua Spradlin, C. Reece, and K. Seo, Supercond. Sci. Technol. 24, 115002 (2011).
- [5] C. Benvenuti, N. Circelli, M. Hauer, Appl. Phys. Lett. 45 (1984) 583.
- [6] C. Benvenuti, Part. Accel. 40 (1992) 43.
- [7] C. Benvenuti, S. Calatroni, I.E. Campisi, P. Darriulat, M.A. Peck, R. Russo, A.-M. Valente, Physica C316, (1999) 153–188 (Elsevier).
- [8] J. Langner, R. Mirowski, M.J. Sadowski, P. Strzyzewski, J. J. Witkowski, S. Tazzari, L. L. Catani, A. Cianchi, J. Lorkiewicz and R. Russo, Vacuum 80 (2006) 1288-1293.
- [9] L. Catani, A. Cianchi, J. Lorkiewicz, S. Tazzari, J. Langner, P. Strzyzewski, M. Sadowski, A. Andreone, G. Cifariello, E. Di Gennari, G. Lamura and R. Russo, Physica C441 (2006) 130-133.
- [10] A. Bendavid, P. J. Martin, R. P. Netterfield, G. J. Sloggett, T. J. Kinder, C., Andrikidis, Journal of Materials Science Letters 12 (1993) 322-323.
- [11] Y. Lifshitz, S. R. Kasi, J. W. Rabalais, and W. Eckstein, Phys. Rev. B 41 (1990) 10468.
- [12] D. K. Brice, J. Y. Tsao, and S. T. Picraux, Nucl. Instrum. Methods Phys. Res., Sect. B 44 (1989) 68.
- [13] A. Anders, Phys. Rev. E 55 (1997) 969.
- [14] J.A. Thornton, Ann. Rev. Mater. Sci. 7 (1977) 239.
- [15] N.A. Marks, Phys. Rev. B 56 (1997) 2441.
- [16] R.L. Boxman, D.M. Sanders and P.J. Martin (editors), "Handbook of Vacuum Arc Science and Technology" (1995), Noyes Publications, Park Ridge, N.J.
- [17] A. Anders, "Cathodic Arcs: From Fractal Spots to Energetic Condensation," Springer (2009).
- [18] M. Krishnan E. Valderrama, C. James, X. Zhao, J. Spradlin, A-M Valente Feliciano, L. Phillips, C. E. Reece, K. Seo, Z. H. Sung, PHYSICAL REVIEW SPECIAL TOPICS - ACCELERATORS AND BEAMS 15, 032001 (2012).